Misaligned Flip-Chip Solder Joints: Prediction and Experimental Determination of Force-Displacement Curves

D. Josell
W. E. Wallace
J. A. Warren
D. Wheeler

National Institute of Standards and Technology,
Gaithersburg, MD 20899

A. C. Powell IV
Massachusetts Institute of Technology,
Cambridge, MA 02139

The results of wetting experiments between eutectic lead-tin solder and copper pads on silicon substrates in geometries relevant to flip-chip applications are presented. Measurements of solder joint dimensions, specifically stand-off height and lateral offset (i.e., misalignment), as functions of the applied force (normal and shear), solder volume and pad diameter are presented. The experimentally-measured force-displacement relationships are compared with predictions obtained from the minimum energy model of the Surface Evolver computer code. For the case of the axisymmetric joint (zero shear) an exact solution to the capillary equations is also presented. The comparison of experimental and modeling results indicates that such models are accurate as well as extremely sensitive means for predicting the geometry of these solder joints.
[DOI: 10.1115/1.1463732]

Introduction

For area-array flip-chip applications, the use of an integrated underfill/solder bump system at the wafer level [1,2] removes the need for subsequent infiltration required by current viscous underfill materials. Unfortunately, the integrated underfill method introduces its own complications, because the viscous underfill retards desired self-alignment of the chip and board. This self-alignment is typically induced by surface energy/area minimization of the molten solder joints (capillary effects). By impeding self-alignment of the die, inclusion of the underfill prior to solder reflow potentially impacts the final solder joint geometry and the corresponding solder joint reliability. This goes against the goal of such underfill materials, which are intended to enhance reliability.

Solder joints in advanced electronics, particularly optoelectronics, are now an integral part of the alignment strategy. This state of affairs has been enabled by the development of advanced modeling codes. Such codes predict the effect of solder joint parameters on flip-chip self-alignment forces, based on minimum energy criterion. Possibly the most widely used modeling code is Surface Evolver [3] (Evolver), which predicts the solder equilibrium shape from user defined parameters such as pad geometry, wetting angles and solder density. However, all these codes, in spite of their sophistication, neglect a wide range of relevant phenomena, which might impact the ultimate solder joint geometry. These include buoyancy-driven convection, Marangoni convection (caused by a tangential surface tension gradient) due to temperature gradients as well as volume changes due to fluxing agents and solidification. For example, Marangoni convection has been used to explain the differences between pure capillary equilibrium and experimental free-surface profiles as well as wetting forces in the wetting balance test with heated oil [4]. In the case of eutectic Sn-Pb solder the differences were too large even for Marangoni flow to provide an explanation [4].

Accurate solder joint design can permit coarse (easy and cheap) chip placement because, if appropriately designed, the solder joints will align the components, with the required accuracy, during processing. The design of solder joints, in particular the selection of solder volume, pad dimension, pad location and pad quantity has been referred to as solder engineering [5]. Determining force-displacement relationships is essential to understanding misalignment of solder joints and thus predicting solder joint integrity.

One of the first attempts at examining the misalignment issue was by Deering and Szekeley [6]. Rotational, horizontal and vertical displacements were examined as well as various pad shapes to determine restoring forces using Surface Evolver. Lin et al. [7] subsequently used Surface Evolver to calculate restoring forces for opto-electronic array type interconnects. The model was used to determine the reaction forces given the misalignment, stand-off height and pad radius. An approximate analytical solution for the stand-off height in the absence of shear force has also been published [8].

Efforts have been made to determine misalignment forces, such as might arise from differential solder volumes, to determine the precision that can be achieved in opto-electronic devices [9]. Researchers studying microelectromechanical systems (MEMS) for microwave applications have achieved control of stand-off height better than 0.1 μm using flip-chip indium bumping technology [10]. The surface tension of glass has also been used to move MEMS devices, relying upon physical stops to define the final position [11]. Other researchers have used eutectic lead-tin solder engineering to actually control the opening angle of MEMS devices to approximately ± 2 deg [12]. This latter study appears to validate the dominance of capillary terms for the MEMS geometry and the fluxless solder technique. However, for the geometry used, the equilibrium shape (i.e., opening angle) is independent of surface tension. Therefore this experiment did not measure the force-displacement relationship for the solder joint.

Researchers have developed analytical solutions that relate the lateral restoring force to the frequency and amplitude decay of a chip oscillating about its equilibrium location on molten solder joints [13]. However, interpretation of the experimental data requires an unphysical surface tension for the Pb60-Sn40 solder of 0.19 J/m [13], less than 50% of other published values for Pb(Sn) eutectic range compositions [4,14]. Interpretation of the same data using a second analytical solution for the oscillatory behavior [15] requires the same unphysical value for the surface tension. The exceedingly low value of the surface tension required to fit the data would seem to indicate that the impact of flow and viscous terms, inherent to understanding the oscillatory problem, is not

Contributed by the Electronic and Photonic Packaging Division for publication in the JOURNAL OF ELECTRONIC PACKAGING. Manuscript received by the EPPD December 19, 2000. Associate Editor: S. M. Heinrich.

adequately understood. This raises questions about the accuracy of force-displacement curves that would be generated using this technique. It should be noted that the solder volumes studied in [13] were 11 mm^3 and 16.5 mm^3, nearly 4 orders of magnitude larger than the smallest studied here. The pad diameters were 3.81 mm, approximately 1 order of magnitude larger than those studied here. Other researchers have modeled the impact of board warpage and variation of solder volume on solder joint shapes in area-array packages [16] or conducted experimental studies of the associated failure of such joints [17].

This paper addresses the wetting behavior of solder in interconnects with the geometry of those found in the wafer-level underfill applications. Fabrication of solder joints with nominal solder volumes as small as 0.0019 mm^3 and pad diameters as small as 0.35 mm, created under a range of shear loads, is described. Post-solidified structures are used to directly obtain force-displacement data for both normal and shear displacements. A Surface Evolver based code for flip-chip geometry is used to generate force-displacement curves for different solder volumes and pad sizes; stand-off and lateral displacements are calculated simultaneously given the normal and shear components of the applied force. In order to validate the numerical Evolver results, an exact solution is developed for zero lateral displacement. Finally, the predicted and experimental results for various sized solder balls and pad radii are compared in order to evaluate the applicability of purely capillary based codes for wafer-level underfill applications, particularly at sub-300μm pad diameter.

Experiments

Each experimental specimen is composed of eight solder joints joining copper pads arranged around a square perimeter (Fig. 1). The pads were deposited on 6 in. silicon wafers by electron beam evaporation of a 5 μm thick layer of copper through a mask. A 30 nm thick titanium intermediate layer was used to retard the rapid si(cu) interdiffusion and enhance adhesion. Masks with 0.64 and 0.35 mm diameter holes were used to fabricate specimens with either 0.64 or 0.35 mm diameter pads, respectively. Individual specimens were obtained by sectioning the 6 in. wafers.

Lateral offsets and stand-off height measurements were obtained from solidified solder joints in this study, under the assumption that these displacements do not vary substantially during solidification. There is a volume decrease associated with solidification of the solder of ~4.5%. However, this corresponds to only a ~1.5% decrease of any linear dimension. In light of this, the lack of a freezing range for the eutectic composition and the small solder joint dimensions (implying minimal convection during the solidification) it is believed that post-solidification joint geometries are reasonably similar to the molten solder joint geometries. Because of inertial considerations, this should certainly be true for the two quantities, stand-off height and lateral offset, measured in this study.

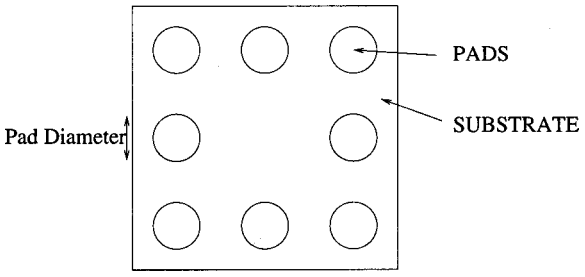

Fig. 1 Schematic of the specimen geometry. Eight copper pads, each 5 μm thick with a ~30 nm Ti intermediate layer on silicon wafer. Two such wafers, with a solder ball between each corresponding pair of pads, were sandwiched together to make each specimen. The pads were all either 0.64 mm or 0.35 mm in diameter. Spacing between pad centers was 5 mm.

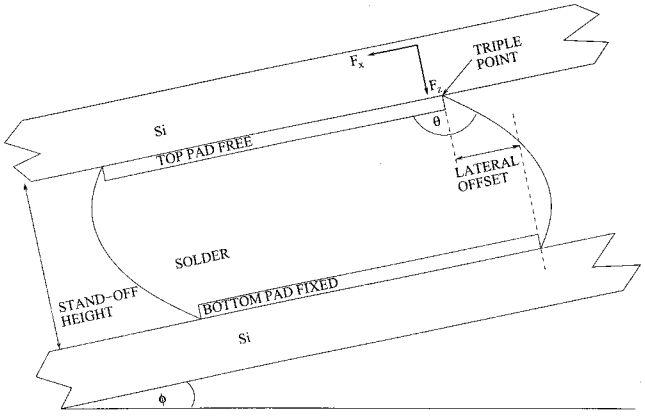

Fig. 2 Shear loading geometry. The stand-off height and lateral offset are defined. Note that the triple point is actually a line where the solid base, liquid solder and ambient vapor come into contact. Note that the contact angle θ will vary along the triple line under non-zero shear loading. In the experiments and modeling, the triple line is not constrained to lie on the perimeter of the pad.

The solder used in these experiments had a eutectic composition (Sn63-Pb37).[1] It came in the form of solder balls with nominal diameters of 15, 10, 9, and 6 mils (380, 255, 225, and 150 μm). Stated uncertainties were +/−1 mil (25 μm). These nominal diameters correspond to volumes of 0.029, 0.0086, 0.0063, and 0.0019 mm^3, respectively. The solder balls were examined by optical microscopy. For the three largest sizes, the average measured diameters were within 5 μm of the nominal diameters, and they exhibited 5 μm or less root-mean-square deviations of individual diameters. These variations are predicted to be insignificant for the experiments described. On the other hand, the nominally 6 mil (152 μm) solder balls were measured to have an average diameter of 163 μm, with a standard deviation of 10 μm. This corresponds to an average volume 25% larger than the nominal value with a standard deviation of approximately 20% for individual solder balls.

Flux, in its undiluted form, was placed on each pad individually. The total volume used on the sixteen pads associated with the two Si specimens to be joined was less than l μl and spread to diameters approximately 3× that of each pad. Flux was thus available in all cases where the solder extruded beyond the Cu pad onto the Si substrate. Larger volumes of flux resulted in local bridging between the Si wafers, beyond that associated with the solder joints, and loss of parallelism of the joined wafers. This was particularly true for the experiments involving stand-off heights of 30 μm and less. One solder ball was manually placed on each corner pad of one wafer and each edge-center pad on the other wafer. The two wafers were separately placed on a hot stage at 210± 10°C (eutectic temperature 183°C) for the time required for the solder balls to melt (typically <5 s). This step ensured that all solder balls were accurately placed on their copper pads. The pads on the two wafers were then aligned with each other and placed on the hostage for the time required to form the solder joints, as determined by the visible shift associated with realignment (typically after 5–10 s). A disk-shaped tantalum weight (mass 1.29 g, diameter 12 mm, height 0.69 mm) was next attached to the center of one wafer using a small amount of the flux. In order to control the applied shear force, the test specimen, with the tantalum weight on top, was reflowed again (10–15 s) and the stage then tilted to the desired angle (Fig. 2). The stage was then

[1]Eutectic solder from Indium Corporation, flux Actiec 2 from Multicore Solders. Corporate names are supplied for completeness of experimental description and does not imply NIST endorsement.

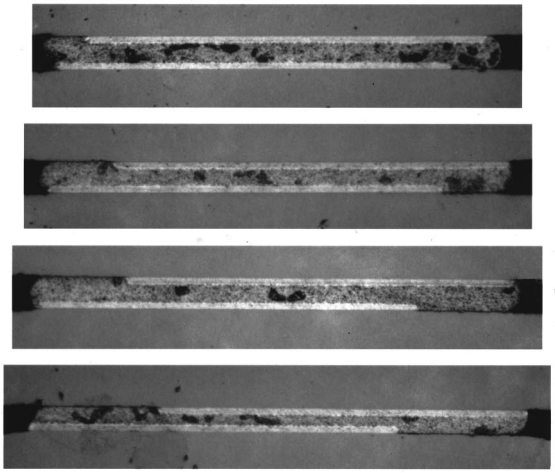

(*a*)

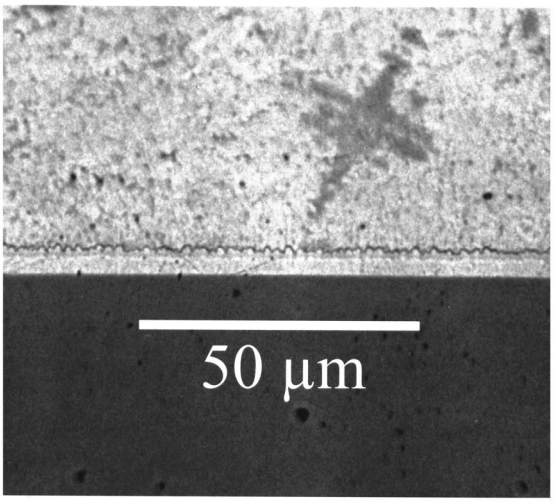

(*b*)

Fig. 3 (*a*) Cross-sectioned solder joints. From top to bottom the shear force is: 34 μN, 68 μN, 100 μN, and 120 μN. Normal forces are approximately 1.95 mN. The pad diameters are all ~350 μm in the cross-sectioned images. (*b*) Close-up of the solder-pad-silicon interfaces showing the intermetallic layer formed between the Pb-Sn eutectic solder and copper pad as well as a Pb-rich dendrite in the solder.

cooled, by running water through internal cooling lines, with the specimen still on it.

The tilt of the stage by the small angle ϕ results in normal and lateral forces where the normal force is given by

$$F_N = \mathrm{mg}\cos(\phi)/n_{\mathrm{jnts}} \tag{1}$$

and the lateral force is given by

$$F_L = \mathrm{mg}\sin(\phi)/n_{\mathrm{jnts}} \tag{2}$$

where g, n_{jnts}, and m are the acceleration due to gravity, the number of solder joints and the weight of the applied mass (including that of the upper silicon wafer), respectively. For the range of tilt angles used, from 0–5 deg away from horizontal, the shear force is very nearly linear in the angle and the normal force is essentially constant (decreasing by less than 0.5% at 5 deg).

Following solder joint solidification, the specimens were mounted in epoxy, using vacuum to ensure infiltration into the area of the joints. After the epoxy had hardened they were cross-sectioned to permit the three solder joints on one edge parallel to the shear direction to be viewed. Polishing was done on a felt

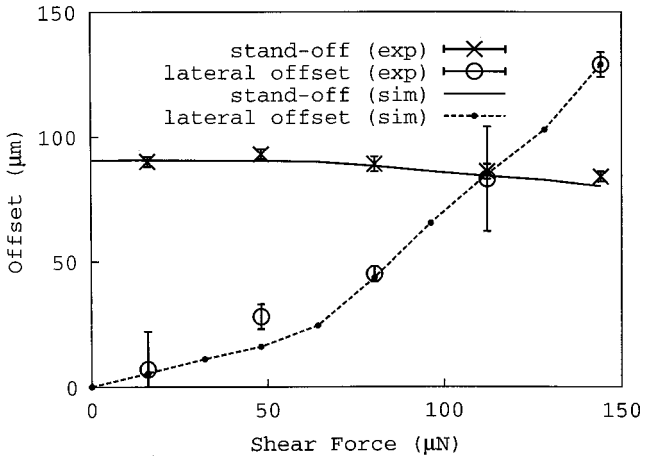

Fig. 4 Experimental and "best fit" simulation for 0.029 mm^3 solder joints and 0.64 mm diameter pads. Experimental data and best fit modeling results are shown for both the stand-off height and lateral offset as functions of the shear force. A portion of the triple line is predicted to move onto the substrate at ~65 μN, causing the kink in the predicted force-displacement curve.

covered wheel using diamond slurry down to 0.25 μm; a final polish in deagglomerated 0.05 μm alumina was extremely helpful in obtaining contrast between the copper pads and the solder. Figure 3(*a*) shows cross-sectioned solder joints formed with 0.35 mm diameter pads, 6 mil solder balls, normal force of 1.95 $\pm$ 0.03 mN (2σ uncertainty) and shear force ranging from 34 μN–120 μN. Two shear displacement values are obtained from the relative lateral displacements of the left edges of the pads and the right edges of the pads (these could differ because of differences in pad diameters or imperfect alignment). A single stand-off value is obtained from the distance between the upper and lower Si/Cu interfaces. These values are averaged with the results from the two other sectioned pads from each specimen to obtain each of the experimental values used in this paper.

Variation of the loads on the eight solder joints in each specimen induced either by inaccurate placement or shift of the centroid during tilting was minimized by the squat shape and accurate centering of the applied weight. Specimens for which the measured stand-off heights of any two pads exceeded 10 μm were discarded. Of forty-five specimens for which data are presented, only two exhibited stand-off heights differing by more than 6 μm; twenty exhibited variation of 2 μm or less. Figure 3(*b*) shows a close-up of typical solder/copper (pad) and copper/silicon interfaces observed in the sectioned specimens. The 1-2 μm thick intermetallic layer formed at the solder/copper interface develops a cellular pattern as it grows into the molten solder. A Pb-rich dendrite is visible in the solidified solder.

The results of all experiments are summarized in the Figs. 4–7. Each plot shows the dependence of the lateral offset and the stand-off height of the solder joint on the applied shear force. Figures 4 and 5 summarize the results for pad diameter 0.64 mm and nominal solder volumes 0.029 and 0.0086 mm^3, representing the 15 and 10 mil solder balls, respectively. Figures 6 and 7 summarize the results for pad diameter 0.35 mm and nominal solder volumes 0.0063 and 0.0019 mm^3, representing the 9 and 6 mil solder balls, respectively. The "best fit" Evolver generated force-displacement curves are also included in all four figures.[2] The shear forces for which Evolver generated data points were obtained are indicated by small filled circles on the lateral offset curve (also for all following figures). The best fit values of the parameters, θ_{Si}

[2]The experimentally determined average diameter of 163 μm has been used in the prediction for the nominally 150 μm solder balls.

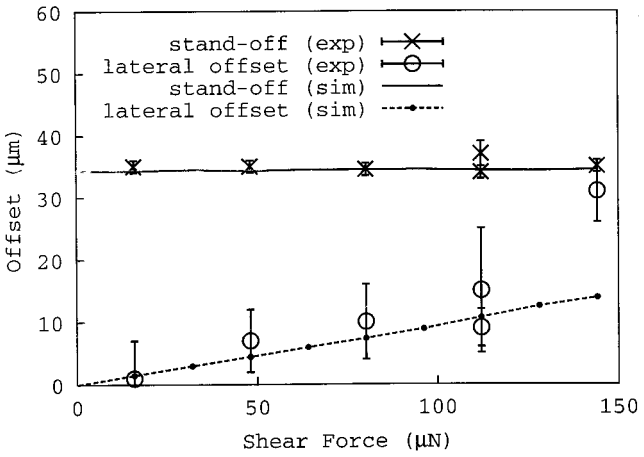

Fig. 5 Experimental and "best fit" simulation for 0.0086 mm^3 solder joints and 0.64 mm diameter pads. Experimental data and best fit modeling results are shown for both the stand-off and lateral offset as functions of the shear force. The triple line lies on the pad perimeter for the range of shear forces shown.

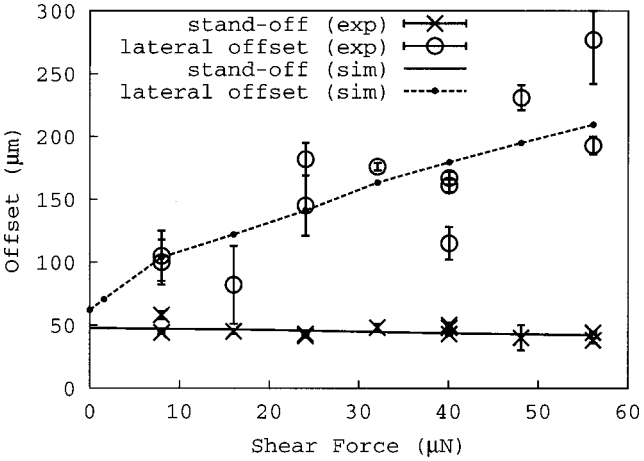

Fig. 6 Experimental and "best fit" simulations for 0.0063 mm^3 solder joints and 0.35 mm diameter pads. Experimental data and best fit modeling results are shown for both the stand-off and lateral offset as functions of the shear force. The triple line lies partly on the substrate for the range of shear forces shown.

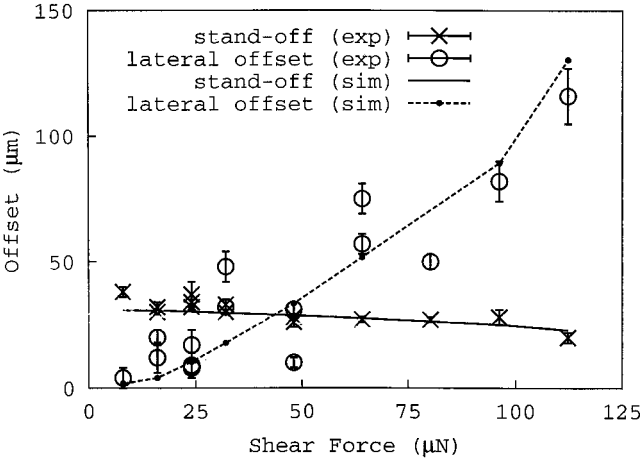

Fig. 7 Experimental and "best fit" simulations for nominal 0.0019 mm^3 solder joints and 0.35 mm diameter pads. Experimental data and best fit modeling results (for actual ~0.0022 mm^3 solder volume) are shown for both the stand-off and lateral offset as functions of the shear force. The triple line wets the substrate at a shear force of ~20 μN.

$=150$deg and $\gamma=0.4$ N/m^2, discussed in the modeling section of this paper, were used for all four figures. For the largest solder volume, the kink in the computed lateral offset at ~65 μN (Fig. 4) is caused by a portion of the triple line (the curve where solder, underlying substrate or pad and vapor meet, see Fig. 2) moving off the pad and wetting the Si substrate. This occurs when the contact angle at that location reaches θ_{Si}. This contrasts with the results in Fig. 5 where the triple line is entirely on the pad perimeter and with Fig. 6 where a portion of the triple line is always on the substrate (thus the nonzero lateral offset for all nonzero shear forces). For the smallest solder volume, wetting of the substrate occurs at ~20 μN shear force (Fig. 7). An additional kink at ~100 μN is possibly associated with development of an instability in the shape of the sheared solder joints.

Other Measurements

In order to model the data, independent values were required for the contact angle on the silicon wafers. Wetting angles of solder on Si with native oxide intact and on evaporated copper pad material (deposited on the Si substrate material without using a mask) were obtained by direct contact angle measurements of the solidified structures obtained with the same eutectic solder, flux and conditions used in the solder joint experiments. The contact angle of the solder on the silicon, θ_{Si}, was found to be 149 ± 3 deg (2σ uncertainty). The value for the contact angle of the solder on the copper thin film pad material, θ_p, was measured to be between 2–5 deg based on both direct contact angle measurement and area of spread.

Modeling

Prediction of vector force-displacement curves for array type interconnects has until now been confined to predicting the force given a displacement e.g. [16]. Unfortunately, the normal and lateral displacements are interdependent, each changing with both the normal and lateral components of the applied force. In theory, equilibrium displacements can be obtained from fixed displacement models using a bracketing technique for the energy. However this is time-consuming, requiring many simulations for each data point, making it especially cumbersome for studies involving a range of geometric and materials parameters. An example of this can be seen in Fig. 8 where many data points are needed to find the minimum at each value of ϕ_{tilt}. Thus, for this study, a Surface Evolver code was developed that determines the equilibrium shape of the flip-chip geometry solder joint, particularly the stand-off and lateral displacements, for a specified applied force. The code, executable using the Surface Evolver computer program [3], can be downloaded for free from NIST at http://www.ctcms.nist.gov/~djl/solder/new.html.

The code was directly applied to modeling the experiments. For aligned pads (zero shear force), an exact solution was also used (Appendix). Both solutions use the following quantities as inputs: solder volume, pad diameter and thickness, solder density, and surface energy and contact angles on the copper pads and silicon substrates. The solutions include capillary forces but ignore convection. Gravitational forces, while included in the general code, were not used here as they are not significant for the solder volumes in question. The minimum mesh refinements for the Evolver solutions were determined by evaluating sequentially more refined meshes until the value of stand-off height converged for the particular specimen geometry. The accuracy of the converged value was confirmed by comparison to the exact solution for the case of aligned pads.

In the experiments described here, the triple line extended to the pad perimeter or beyond in all cases. Analogously, in the Evolver modeling, for the shearing conditions studied, the contact angle always exceeded θ_p on both the trailing and leading edges of the sheared solder drop. Based on both these results, the jump in height from the silicon to the pad was ignored and a flat plane with variable contact was used for the Evolver geometry. It re-

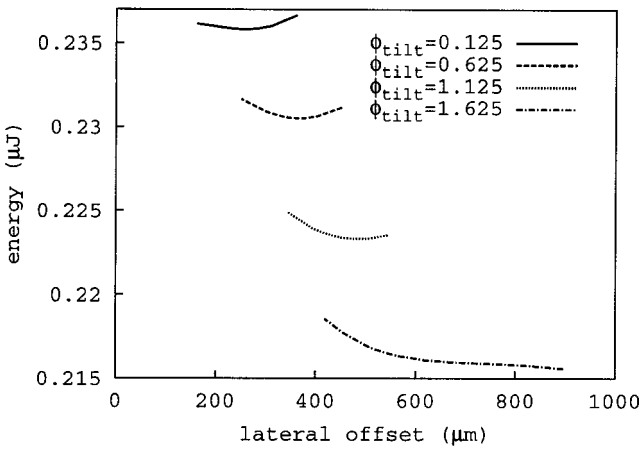

Fig. 8 Energy contours around the minimum energy regions using data points from many simulations. At $\phi_{tilt}=1.625$ the shear force has reached a saddle point indicating an increase in ϕ_{tilt} would lead to failure of the sample.

mained necessary to correct for the volume of the two pads in each joint. This was accomplished by increasing the solder volume in the models by the volume of the pads.

The Evolver solution procedure does not require user interaction and involves using an energy bracket at each stage of the mesh refinement to move the displacement parameters [18]. With the understanding that the pad is fully wetted, the total energy for the solder configuration (see Fig. 2) is given by,

$$E=F_x x_0+F_z h+\int_S \gamma dS-2\left[\pi r_P^2\gamma\cos(\theta_p)+\gamma\cos(\theta_{Si})\int_0^{2\pi}(r_{TL}^2(\phi)-r_p^2)d\phi\right] \quad (3)$$

The first two terms in Eq. (3) equal the potential energy of the applied vector force **F** with x_0 and h the lateral offset and stand-off height. The third term equals the energy of the solder (liquid/vapor) surface S, with free energy γ. This surface is the only faceted (discretized) surface in the Evolver calculations. The term in square brackets equals the change of system energy associated with wetting the entire Cu pad as well as the region of the Si substrate within the triple line. Gravitational potential energy is neglected here. The symbols r_p and r_{TL} are the radius of the pad and the distance from the center of the pad to the triple line, respectively. Young's equation has been used to relate the free energy difference between the wetted and unwetted Si and Cu surfaces to the wetting angles θ_{Si} and θ_p and the solder surface tension γ. The overall factor of 2 reflects the symmetry of the upper and lower surfaces when gravity is neglected. The volume of the solder is maintained as a constant with the volume of the pads included. Note that, when the local contact angle θ falls between the wetting angles on the Cu pad and Si substrate, $\theta_{Si}\geq\theta\geq\theta_p$, the triple line is pinned on the pad perimeter at that location. Wetting of the substrate occurs when θ equals θ_{Si} (see Fig. 2).

Table 1 shows the results of a χ^2 analysis obtained by allowing the surface tension, γ, and the contact angle on the silicon, θ_{Si}, to be simultaneous fitting parameters for all the force-displacement data from the four geometries. Every experimental lateral offset and stand-off data point is included. The experimentally measured volume, rather than the nominal value, was used for the modeling with the smallest solder balls. Experimental uncertainty values for each data point were used for normalizing. The best fit is obtained for values of $\theta_{Si}=150$ deg and $\gamma=0.4$ N/m^2, although a continuum of values with increasing (decreasing) θ_{Si} and decreasing-(increasing) γ also fits the data reasonably well. The consistency of the optimal angle and the experimentally obtained value of 149 deg already mentioned is noteworthy, as is the fact that the associated value for γ is reasonable.

Table 1 Least squares fitting of all experimental data

χ^2	$\theta_{Si}=140°$	150°	160°
$\gamma=0.3$ N/m^2	499.8	212.3	93.5
0.35	159.0	36.1	9.3
0.4	35.4	6.7	13.8
0.45	8.6	17.0	32.8

In order to understand the trends in the χ^2 fit the following should be understood. First, fitting of data where the triple line is fully on the perimeter (i.e., the solder does not wet the substrate) will give a quality of fit that is independent of θ_{Si}. Therefore, in the χ^2 analysis, this subset of the experimental data only affects the selection of the optimal value of γ. This data corresponds to low shear forces (less than the value for the kink indicating initial wetting of the substrate) and/or small solder volume. The shear force at which the kink occurs depends on both θ_{Si} and γ. Also, once the triple line moves onto the substrate, the slope of the force-displacement (lateral offset) curve depends on both γ and θ_{Si} as a result of the Young-Laplace equation.

Discussion

These results demonstrate the sensitivity of the experiments and the model to the shear force and to the contact angle at which the solder first wets the substrate (leading to a solder joint whose triple line is not confined to the perimeter of the pad). A substantial decrease of stiffness is associated with this event. Figure 9 shows the data for the largest solder balls with predictions obtained by varying γ for fixed $\theta_{Si}=150$deg. The kink in the force-displacement curves occurs when the triple line leaves the perimeter of the pad and wets the substrate. Figure 10 shows the corresponding fraction of the triple line on the substrate for each value of γ. Figure 11, in which θ_{Si} is varied while γ is held constant, yields curves similar to those shown in Fig. 9 as expected from Young's equation. Note that the results for $\theta_{Si}=150$ deg and $\theta_{Si}=160$ deg are identical for shear forces below 50 μN because the solder remains entirely on the pad.

The experimental results for the smallest solder balls exhibited considerable variance, which can be explained by the scatter in the volume of the samples (standard deviation 20%). This effect is

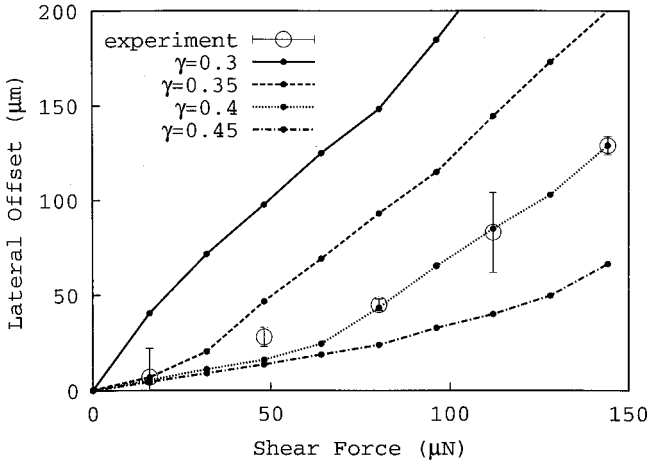

Fig. 9 Comparison of experimental data and force-displacement curves for 0.029 mm^3 solder joints and 0.64 mm diameter pads holding $\theta_{Si}=150$ deg and varying γ

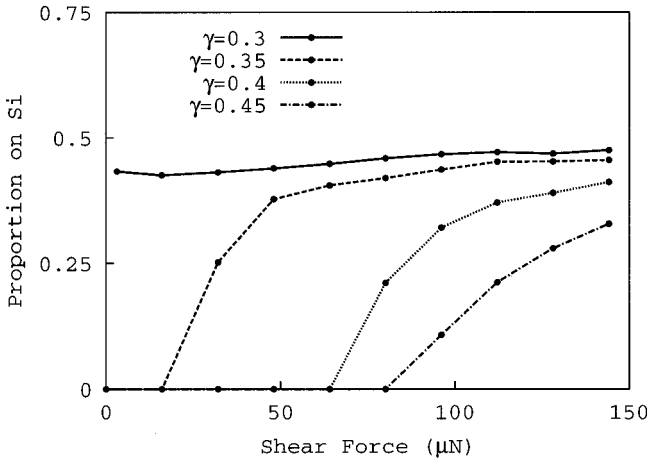

Fig. 10 Proportion of the triple line on the substrate for 0.029 mm^3 solder joints and 0.64 mm diameter pads holding θ_{Si} = 150 deg and varying γ. The critical point, at which the solder wets the substrate, corresponds to the change in slope of the force-displacement curves in Fig. 9.

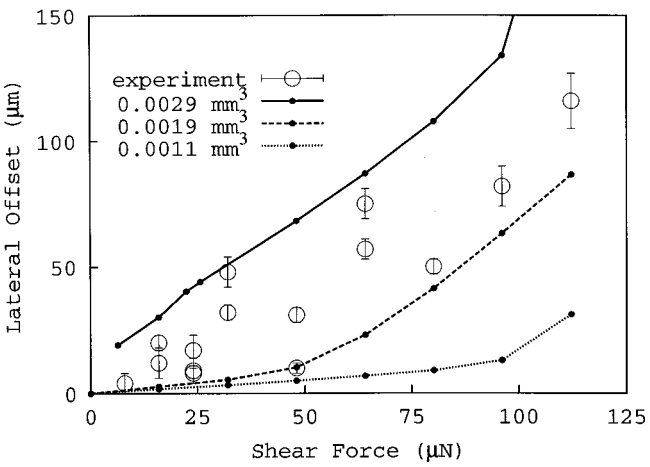

Fig. 12 Lateral offset for 0.35 mm pads, γ=0.4 N/m^2 and θ_{Si} = 150 deg for solder balls of varying diameter. The experimental distribution is consistent with the known variation of solder ball volumes.

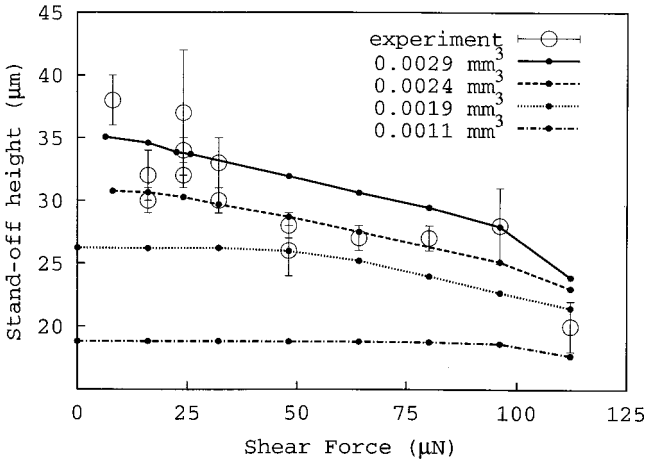

Fig. 13 Stand-off height for 0.35 mm pads, γ=0.4 N/m^2 and θ_{Si}=150 deg for solder balls of varying diameter. Data corresponds to that in Fig. 12.

accentuated by the critical dependence of the displacements on volume for these particular experimental conditions. Simulations were made for solder balls with diameters of 125 μm, 150 μm, 162 μm, and 175 μm. The 125 μm and 150 μm diameter solder balls triple lines remained on the pad perimeter. The 162 μm solder balls wetted the Si substrate at 25 μN (not shown). The 175 μm solder balls wetted the substrate for all shear forces (see Fig. 12). The average diameter of the solder balls, 160 μm, places the experimental volume right in this transition region. The cross-sectioned solder joints indicated that solder joints exhibiting small lateral offsets had remained fixed to the pad perimeter while those with large offsets had wetted the silicon (see Fig. 3), agreeing with theory. The simulations for 162 μm diameter were used in the best fit analysis because this value of the diameter best matched the experimental diameter measurements; Fig. 7, 12, and 13 show that the 162 μm diameter results also fit the force-displacement data the best. It should be noted that some of the volume variance also might be due to voids in the solder balls, which were observed in a number of cross-sectioned solder joints.

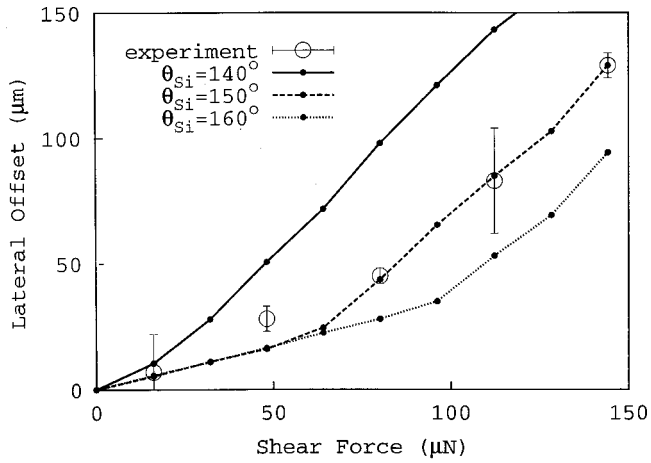

Fig. 11 Comparison of experimental data and force-displacement curves for 0.029 mm^3 solder joints and 0.64 mm diameter pads holding γ=0.4 N/m^2 and varying θ_{Si}

Conclusion

This paper presented the wetting behavior of solder in flip-chip geometry interconnects. A Surface Evolver based code for flip-chip geometry was used to generate force-displacement curves for different solder volumes and pad sizes. The experimental results and those obtained from Surface Evolver are consistent. A computer code that permits solder joint displacements to be determined given applied forces, developed in this effort, has been shown to be accurate as well as more convenient than codes that solve for forces given displacements.

The motivation for this study was a need to assess the validity of using only static surface tension theory for use in understanding flip-chip misalignment. The qualitative and quantitative agreement for the substrate wetting and optimized parameter values (γ, θ_{Si}) suggest that static theory does predict the force-displacement relationships in these experiments quite well. The value of θ_{Si} is near the experimental measurement and γ is consistent with values from the literature. It is therefore evident that, for the dimensions and materials used in this study, only capillary and gravitational forces are required to accurately predict solder joint stand-off heights and lateral offsets given applied shear and normal forces.

Acknowledgments

The authors thank L. Smith for metallography. This project was supported in part by NIST's Advanced Technology Program.

Appendix on Exact Solution

An analytic solution for the axisymmetric hanging liquid droplet suspended between two fixed plates exists when gravity is neglected. This problem has been solved in different contexts, including creep in a wire with bamboo structure [19], a general treatment [20] and liquid infiltration between glass plate with nonwetting regions [21].

The energy E of a loaded axisymmetric drop can be expressed as

$$E=\int_{-L/2}^{L/2} 2\pi r(z)\gamma\sqrt{1+(dr/dz)^2}dz-FL \tag{4}$$

where F is the applied load, L is the height of the drop, $r(z)$ is the radius of the drop as a function of the height coordinate z, and γ is the liquid-vapor surface energy. The volume of the drop V is fixed, yielding

$$V=\int_{-L/2}^{L/2}\pi r(z)^2dz. \tag{5}$$

The shape of the drop $r(z)$ and height L that minimizes E for constant V is obtained using the method of Lagrange multipliers. Defining

$$\psi=E-\lambda V \tag{6}$$

with λ the Lagrange multiplier and minimizing ψ yields the equation

$$F=\frac{2\pi\gamma r(z)}{\sqrt{1+(dr/dz)^2}}-\pi\lambda r^2(z) \tag{7}$$

This expresses a balance of normal forces at the boundary, for λ identified as the pressure. Equation (7) can be used to obtain expressions for L and V expressed as integrals from the radius at the top of the drop, r_t, to the radius at the center, r_c. Expressions for r_c and r_t can also be obtained from Eq. (7) by noting that $dr/dz=0$ when $r=r_c$ and $\sqrt{1+(dr/dz)^2}=1/\tan\theta$ when $r=r_t$, where θ is the contact angle at the upper surface.

There are two possible constraints, either fixed r_t (on the pad) or fixed θ (off the pad). For the latter case, defining $\tilde{F}=F/{r_c}^2\pi\lambda$, $\tilde{q}\equiv\gamma/\lambda r_c$, $x\equiv r_t/r_c$, and introducing a scaled coordinate $u=r/r_c$, one can obtain

$$2\tilde{q}=\frac{1-x^2}{1-x\sin\theta} \tag{8}$$

and

$$\tilde{F}=2\tilde{q}^2-1=\frac{x(\sin\theta-x)}{1-x\sin\theta} \tag{9}$$

from the expressions for r_c and r_t. Using these definitions, the integral expressions for L and V can be written

$$L=2r_c\int_x^1 du\,\frac{(2\tilde{q}-1+u^2)}{\sqrt{(u-1)(u+1)(2\tilde{q}-u-1)(2\tilde{q}+u-1)}}\equiv r_cI_1(x) \tag{10}$$

and

$$V=\pi r_c^3\int_x^1 du\,\frac{u^2(2\tilde{q}-1+u^2)}{\sqrt{(u-1)(u+1)(2\tilde{q}-u-1)(2\tilde{q}+u-1)}}\equiv r_c^3I_2(x) \tag{11}$$

where $\tilde{q}$ is the function of x given by Eq. (8). Equations (10) and (11) yield

$$\left(\frac{L}{I_1(x)}\right)^3=\frac{V}{I_2(x)} \tag{12}$$

which can be solved for x using a standard root finder or tabulated Elliptic Integrals.

References

[1] Johnson, C. D., and Baldwin, D. F., 1999, Proceedings of the 1999 Electronic Components and Technology Conference, 950.
[2] Johnson, C. D., Baldwin, D. F., 1999, International Symposium on Advanced Packaging Materials, 73.
[3] Brakke, K. A., *Surface Evolver Manual*, University of Minnesota Press. http://www.susqu.edu/facstaff/b/brakke/evolver/evolver.html.
[4] Moon, K. W., Boettinger, W. J., Williams, M. E., Josell, D., Murray, B. T., Carter, W. C., Handwerker, C. A., 1996, ASME J. Electron. Packag., **118**, p. 174.
[5] Lee, Y. C., and Basavanhally, N., 1994, J. Met., **46**, p. 46.
[6] Deering, S. E., and Szekely, J., 1994, J. Electron. Mater., **23**, p. 1325.
[7] Lin, W., Patra, S. K., and Lee, Y. C., 1995, IEEE Trans. Compon. Packag. Manuf. Technol., Part B, **18**, p. 543.
[8] Heinrich, S. M., Schaefer, M., Schroeder, S. A., and Lee, P. S., 1996, ASME J. Electron. Packag., **118**, p. 114.
[9] Lee, T. S., Choi, T. P., and Yoo, C. D., 1997, ASME J. Electron. Packag., **119**, p. 119.
[10] Harsh, K. F., Su, B., Zhang, W., Bright, V. M., and Lee, Y. C., 2000, Sens. Actuators, **80**, p. 108.
[11] Syms, R. R. A., 1998, Sens. Actuators A, **65**, p. 238.
[12] Harsh, K. F., Bright, V. M., and Lee, Y. C., 1999, Sens. Actuators, **77**, p. 237.
[13] Landy, M., Patra, S. K., and Lee, Y. C., 1991, Manufacturing Processes and Materials Challenges in Microelectronic Packaging, AMD-131/EEP-1, 49.
[14] Park, J. Y., Kang, C. S., and Jung, J. P., 1999, J. Electron. Mater., **28**, p. 1256.
[15] van Veen, N., 1999, ASME J. Electron. Packag., **121**, p. 116.
[16] Thompson, T. B. Subbarayan, G., James, R., and Renken, F. P., private communication.
[17] Amagai, M., 1999, Microelectronics Reliability, **39**, p. 1365.
[18] Press, W. H., Flannery, B. P., Teukolsky, S. A., and Vetterling, W. T., 1988, *Numerical Recipes in C*, Cambridge University Press, 2nd edition.
[19] Josell, D., 1993, Acta Metall. Mater., **41**(7), p. 2179.
[20] Carter, W. C., 1988, Acta Metall., **36**, p. 2283.
[21] Silver, J., Mi, Z. H., Takamoto, K., Bungay, P., Brown, J., and Powell, A., 1999, J. Colloid Interface Sci., **219**, p. 81.